European Journal of Radiology 117 (2019) 126–131

Contents lists available at ScienceDirect

European Journal of Radiology

journal homepage: www.elsevier.com/locate/ejrad

Research article

Can texture features improve the differentiation of infiltrative lung adenocarcinoma appearing as ground glass nodules in contrast-enhanced CT?

Chen Gao[a,b,1], Ping Xiang[a,b,1], Jianfeng Ye[a,b], Peipei Pang[c], Shiwei Wang[a,b], Maosheng Xu[a,b,*]

[a] The First Clinical Medical College of Zhejiang Chinese Medical University, Hangzhou, China
[b] Department of Radiology, The First Affiliated Hospital of Zhejiang Chinese Medical University, Hangzhou, China
[c] GE Healthcare Life Sciences, Hangzhou, China

ARTICLE INFO

Keywords:
Texture feature
Lung adenocarcinoma
Ground glass nodule

ABSTRACT

Objectives: To investigate the validity and efficacy of comparing texture features from contrast-enhanced images with non-enhanced images in identifying infiltrative lung adenocarcinoma represented as ground glass nodules (GGN).

Materials and methods: A retrospective cohort study was conducted with patients presenting with lung adenocarcinoma and treated at a single centre between January 2015 to December 2017. All patients underwent standard and contrast-enhanced thoracic CT scans with 0.5 mm collimation and 1 mm slice reconstruction thickness before surgery. A total of 34 lung adenocarcinoma patients (representing 34 lesions) were analysed; including 21 instances of invasive adenocarcinoma (IAC) lesions, 4 instances of adenocarcinoma in situ (AIS) lesions, and 9 minimally invasive adenocarcinoma (MIA) lesions. After radiologists manually segmented the lesions, texture features were quantitatively extracted using Artificial Intelligence Kit (AK) software. Then, multivariate logistic regression analysis based on standard and contrast-enhanced CT texture features was employed to analyse the invasiveness of lung adenocarcinoma lesions appearing as GGNs. A receiver operating characteristic (ROC) curve analysis was used to evaluate the performance of those models.

Results: A total of 21 quantitative texture features were extracted using the AK software. After dimensionality reduction, 5 and 3 features extracted from thin-section unenhanced and contrast-enhanced CT, respectively, were used to establish the model. The area under the ROC curve (AUC) values for unenhanced CT and enhanced CT features were 0.890 and 0.868, respectively. There was no significant difference (P = 0.190) in the AUC between models based on non-enhanced and contrast-enhanced CT texture features.

Conclusion: Compared with unenhanced CT, texture features extracted from contrast-enhanced CT provided no benefit in improving the differential diagnosis of infiltrative lung adenocarcinoma from non-infiltrative malignancies appearing as GGNs.

1. Introduction

As of 2017 bronchogenic cancer was reported as the second-most common type of cancer overall, and the top-ranking cause of cancer-related deaths in the United States [1]. According to the guidelines from the International Association for the Study of Lung Cancer/American Thoracic Society/European Respiratory Society (IASLC/ATS/ERS) in the 2011 [2]; if adenocarcinomas in situ (AIS) and minimally invasive adenocarcinomas (MIA) were completely resected, survival rates could reach 100%. As evident in recent studies, AIS and MIS often appear as ground glass nodules (GGNs) on CT imaging. However, invasive adenocarcinoma (IAC) also represents itself as GGNs or solid nodules on imaging [3–6]. Therefore, a reliable method to differentiate AIS/MIA from IAC, which can both be visualized as GGNs, has great potential in guiding treatment of bronchogenic carcinoma.

A GGN is defined as a hazy, hyperdense region that does not obscure bronchovesicular structures on lung windows [7–9]. CT is often equipped to evaluate the invasion of GGNs in clinical practice, and conventional CT features are frequently employed to evaluate the characteristics of GGNs, such as size, density, and shape [10]. However,

* Corresponding author at: Department of Radiology, The First Affiliated Hospital of Zhejiang Chinese Medical University, 54 Youdian Road, Hangzhou, China.
E-mail address: xums166@zcmu.edu.cn (M. Xu).
[1] These authors contributed equally to this work.

https://doi.org/10.1016/j.ejrad.2019.06.010
Received 9 April 2019; Received in revised form 27 May 2019; Accepted 11 June 2019

a reliable diagnosis relying on these morphological features from unenhanced CT images alone remains subpar. Particularly, delineating an AIS/MIA from IAC solely using the presence of a GGN remains a distinctive challenge [11,12].

In light of this challenge, a suggestion to improve diagnostic accuracy using contrast-enhanced CT was proposed. Contrast-enhanced CT has proved its value in the diagnosis of solid malignant tumours, such as lung cancer, brain tumours, and hepatocellular carcinomas. Yet, whether contrast-enhanced CT imaging is sufficient to differentiate IAC from AIS/MIA remains controversial. Theoretically, GGNs are filled with gas. Therefore, the mean CT value in contrast enhanced images can vary due to patients' respiratory status, and the partial volume effect of image acquisition. However, investigating morphological features from enhanced CT images can also be of value in the diagnosis of AIS, MIA, and IAC as evidenced in the study performed by Gao et al. [13].

With continual advances in computer technology, texture features have been quantitatively extracted from medical images, such as the grey-level co-occurrence matrix (GLCM) and grey-level run-length matrix (RLM) [14]. Using these methods, many studies have evaluated the invasion of GGNs [15–17]. For example, Chae et al. [15] retrospectively analysed the potential predictive power of texture features extracted from unenhanced CT images to distinguish IAC from preinvasive nodules; both of which manifest as part-solid GGNs on CT images. However, the majority of previous studies have only extracted texture features from non-enhanced CT images. Only a small number of studies have reported the true effectiveness of texture features extracted from contrast-enhanced CT images for discrimination between AIS/MIA and IAC manifested as GGNs.

The purpose of our study was to investigate the reliability of texture features extracted from contrast-enhanced CT images to determine the invasiveness of GGNs.

2. Materials and methods

2.1. Patients

This retrospective study was approved by our institutional review board and the informed consent requirement was waived. Between January 2015 and December 2017, a total of 34 patients with primary pulmonary adenocarcinoma manifesting as GGNs were involved in this study. The inclusion criteria were as follows: (1) pathological specimens were obtained after surgical resection; (2) unenhanced thin-section CT and enhanced thin-section CT scans were both performed at the same visit; (3) biopsy, radiotherapy, chemotherapy or surgical resection were not performed for lesions before CT examination; and (4) the interval between CT examination and surgery was within 30 days. The exclusion criteria were as follows: (1) severe respiratory artifacts on CT images; (2) a history of lung surgery; and (3) lesions larger than 3 cm at the in any axis.

2.2. Image acquisition and analysis

All images were obtained with an Aquilion ONE (Toshiba Medical Systems, Tokyo, Japan) CT scanner. The main scanning parameters were as follows: tube voltage, 120 kVp; tube current, 200 mAs; collimation, 0.5 mm × 64; matrix 512 × 512; reconstruction slice thickness, 1 mm; and rotation time, 0.4 s. The reconstruction kernel was FC51 for unenhanced CT images and FC13 for enhanced CT images. The dose of contrast media was 1 mL/kg, and the speed of administration was 3 mL/s.

Lung nodules were divided into three types, including pure GGNs, subsolid nodules, and solid nodules, by two radiologists (one with 10 years of experience and another with 3 years of experience in chest radiology) based on thin-section, unenhanced CT images. Pure GGNs were defined as nodules that were visible in the lung window but not in the mediastinal window. Solid nodules were defined as nodules that were visible in both the lung window and mediastinal window. All lung nodules were confirmed by two radiologists to reach a consensus. For situations of discrepancy between the two radiologists, a professor of radiology with 27 years of experience in pulmonary radiology evaluated the nodules to break the tie. The size of each nodule was defined as the maximum length of the lesion in any axis using the lung window in thin-section CT images [18]. All measurements were made on transverse sections by two radiologists with a consensus agreement.

2.3. Region of interest segmentation and feature extraction

All layers of thin-sectioned CT images were manually segmented on ITK-SNAP 3.6.0 (www.itksnap.org). Both unenhanced CT images, and enhanced CT images were evaluated. A total of 21 texture features were quantitatively analysed using AK software (Analysis Kit, GE Healthcare, US). The extracted features included single-order parameters, such as histograms and morphologic features, along with higher-order parameters, such as the grey-level co-occurrence matrix (GLCM). The extracted texture features were standardized to remove the unit limits of each feature. Dimension reduction was performed as follows: first, analysis of variance (ANOVA) and the Mann-Whitney *U* test (MW) was performed. Second, univariate logistic regression and statistically significant features ($P < 0.05$) were chosen. Finally, features with a correlation coefficient greater than 0.9 were removed to eliminate redundancy.

2.4. Intra- and inter-observer agreement

The intra- and inter-observer agreement for feature extraction were evaluated with the intra-class correlation coefficient (ICC). Initially, 20 random CT images were chosen for the region of interest (ROI) segmentation and feature extraction. ROI segmentation was performed independently by two experienced radiologists. The intra-observer ICC was computed by comparing two feature extractions conducted by reader A (with 10 years of experience in pulmonary CT). The inter-observer ICC was computed by comparing feature extractions performed by a second reader (reader B, with 3 years of experience in pulmonary CT) with the first feature extraction of reader A. An ICC was greater than 0.75 was considered in good agreement, and the remaining image segmentations were performed by reader A.

The entire process of data acquisition, lesion segmentation, feature extraction, feature selection, and model construction in this study was shown in Fig. 1.

2.5. Statistical analysis

The variables with a univariate P-value < 0.05 were considered as candidate predictors for the multivariate logistic model based on features extracted from unenhanced CT images and enhanced CT images. The performance of these models was evaluated by receiver operating characteristic (ROC) curve analysis. Statistical analyses were performed using SPSS 19 and R software (version 3.5.1). Logistic regression and ROC curve analysis were performed using the "glm", "pROC" and "ROC.TEST" software packages for R.

3. Results

3.1. Basic information

A total of 34 GGNs from 34 patients were included in this study. Of the 34 patients, 12 were male, and 22 were female. The mean age of the patients was 56.15 ± 7.99 years (range = 48–79 years). The mean size of the lesions was 13.98 ± 5.38 mm (range = 6.35–26.40 mm).

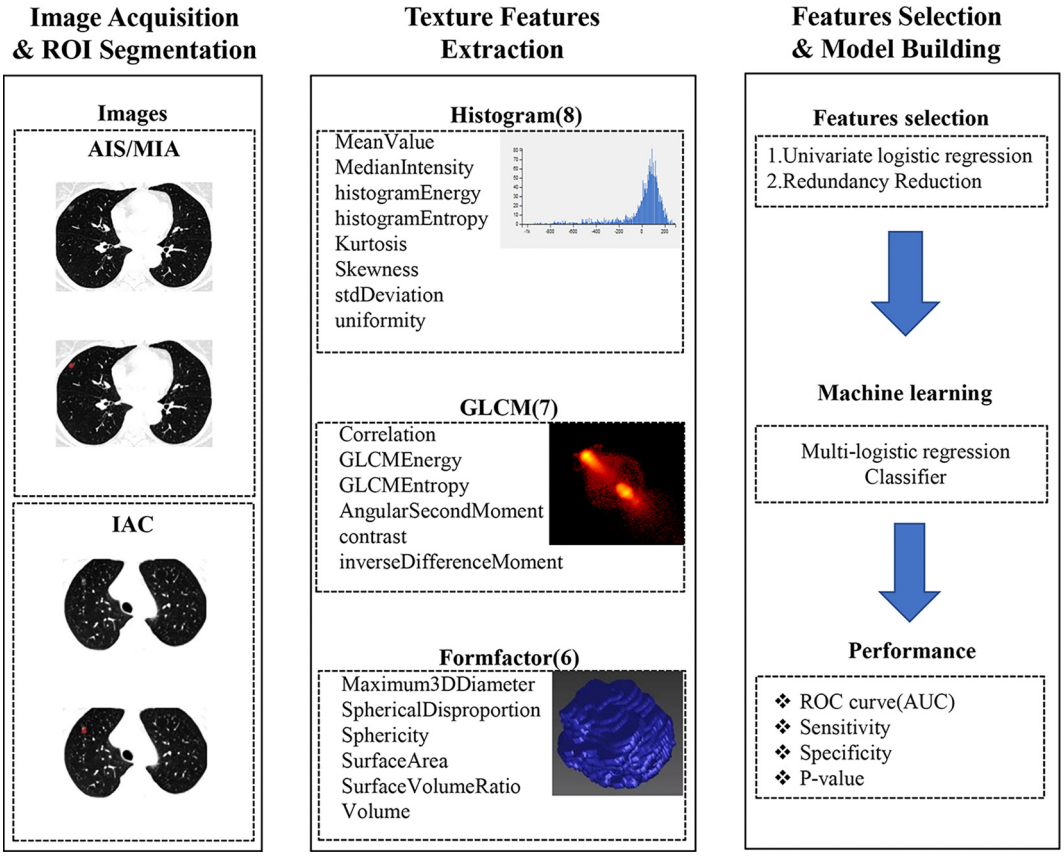

Fig. 1. The process from imaging to modelling.
The entire process of this study included image acquisition, lesion segmentation, feature extraction, feature selection, and model building. Histogram, grey-level co-occurrence matrix (GLCM) and formfactor features were extracted by AK software.

3.2. Inter-observer and intra-observer reproducibility for texture feature extraction

The intra-observer ICC calculated based on two measurements from reader A ranged from 0.854 to 0.964. The inter-observer agreement between the two readers ranged from 0.804 to 0.912. The results indicated favourable intra- and inter-observer reproducibility of feature extraction.

3.3. Feature analysis

After univariate logistic regression and removing redundancies, five features, including “MedianIntensity”, “Uniformity”, “GLCMEnergy”, “AngularSecondMoment” and “Volume” varied significantly between AIS/MIA and IAC on non-enhanced thin-section CT images (Fig. 2). Three features, including “Uniformity”, “GLCMEnergy” and “Volume” varied significantly between AIS/MIA and IAC on enhanced thin-section CT images as well (Fig. 2). The statistically significant features are listed in Table 1.

3.4. Model development and analysis

The first multivariate logistic regression model used selected features from non-enhanced CT images. The sensitivity, specificity, and area under the ROC curve (AUC) were 84.6%, 76.2% and 0.890 (95% CI 0.784–0.996), respectively (Table 2, Fig. 3). The second multivariate logistic regression model used selected features from enhanced CT images with a sensitivity, specificity, and AUC of 84.6%, 76.2% and 0.868 (95% CI 0.750–0.986), respectively (Table 2, Fig. 3). The performance of quantitative features extracted from non-enhanced CT and enhanced CT images for diagnosing invasive adenocarcinoma manifesting as GGNs was not significantly different (P = 0.1897, z = 1.311).

4. Discussion

In the present study, two key features were compared. Specifically, the use of features extracted from enhanced, and non-enhanced CT images for distinguishing between AIS/MIA or IAC manifesting as GGNs, was evaluated. In addition, the value of texture features extracted from non-enhanced features was also evaluated for potential use in diagnosis. To reduce the CT partial volume effect, non-enhanced and enhanced CT images were acquired with a thin-section reconstruction algorithm in our study. This method allowed for more detailed evaluation in comparison with thick-section CT images.

Our study not only included histograms and morphological features, but also higher-order texture parameters such as GLCM. GLCM parameters show the relationship between grey levels in an image and are widely used to reveal the texture of lung cancer on CT images [19,20]. For example, Coroller et al. [21] showed that a model including GLCM, wavelet features, and other higher-order texture parameters could predict distant metastasis of lung adenocarcinoma. Due to the heterogeneity of tumours, the inclusion of these texture features may be useful for identifying the invasion of lung adenocarcinoma.

In this study, five features from unenhanced CT images were included in a diagnostic model. The sensitivity, specificity, and AUC were 84.6%, 76.2% and 0.890 (95% CI 0.784–0.996) respectively. These features included “MedianIntensity”, “Uniformity”, “GLCMEnergy”, “AngularSecondMoment” and “Volume”. There have been similar studies conducted throughout the world. Son et al. [17] retrospectively illustrated the potential predictive power of texture features for differentiating IAC from AIS/MIA. CT images of 191 GGNs were

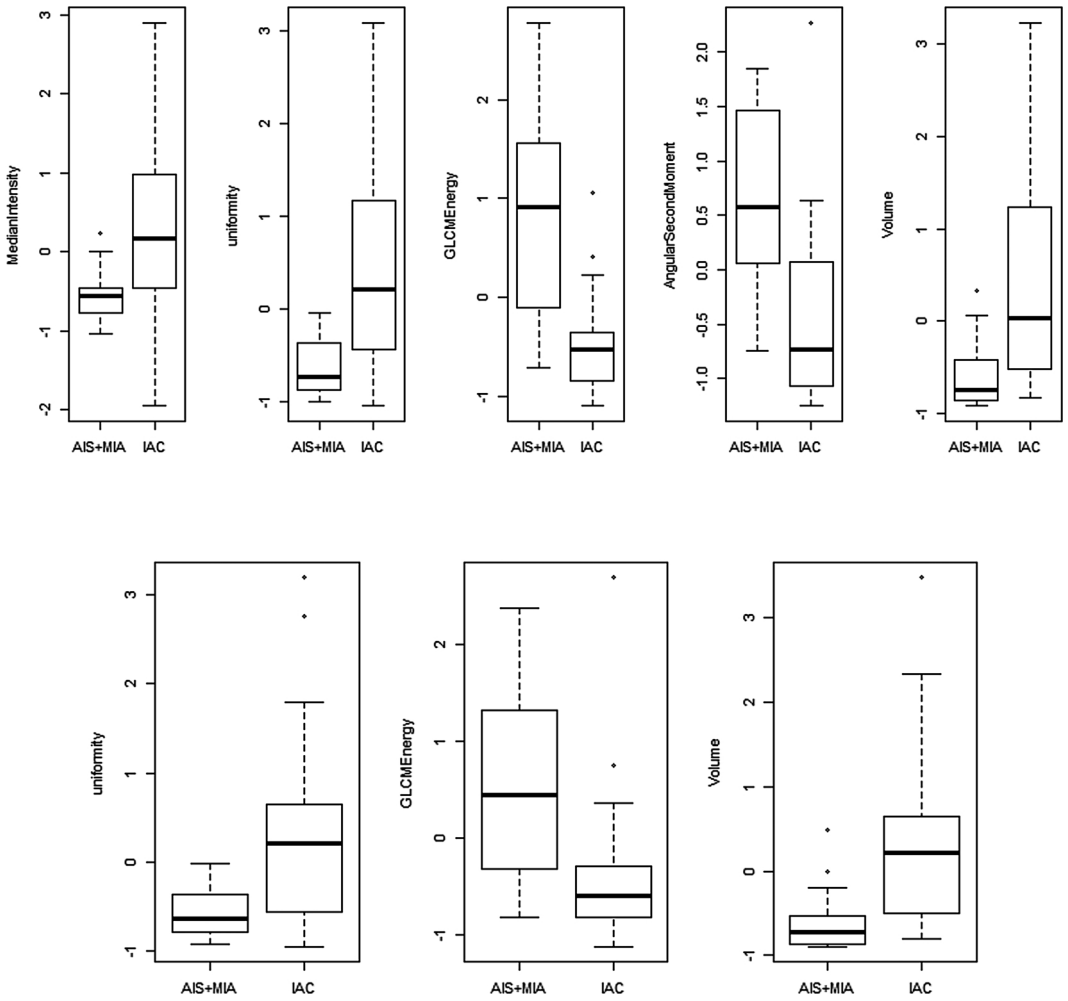

Fig. 2. Key features after univariate logistic regression and removing redundancies.
On the upper line, five features, including "MedianIntensity", "Uniformity", "GLCMEnergy", "AngularSecondMoment" and "Volume", varied significantly between AIS/MIA and IAC on non-enhanced thin-section CT images. On the lower line, three features, including "Uniformity", "GLCMEnergy" and "Volume", varied significantly between AIS/MIA and IAC on enhanced thin-section CT images.

Table 1
Selected features of lung adenocarcinoma with GGNs (n = 34).

Characteristic	AIS/MIA (n = 13)	IAC (n = 21)	P value
Unenhanced CT			
MedianIntensity	−0.52 ± 0.38	0.32 ± 1.13	0.004
Uniformity	−0.61 ± 0.32	0.38 ± 1.09	0.001
GLCMEnergy	0.76 ± 1.12	−0.47 ± 0.53	0.002
AngularSecondMoment	0.69 ± 0.86	−0.43 ± 0.84	0.001
Volume	−0.58 ± 0.40	0.36 ± 1.10	0.001
Enhanced CT			
Uniformity	−0.56 ± 0.31	0.35 ± 1.12	0.002
GLCMEnergy	0.59 ± 0.98	−0.36 ± 0.84	0.005
Volume	−0.57 ± 0.42	0.35 ± 1.10	0.002

Note: Data are represented as mean ± standard deviation.
AIS: adenocarcinoma in situ, MIA: minimally invasive adenocarcinoma, IAC: invasive adenocarcinoma. Classified according to the international multidisciplinary lung adenocarcinoma classification system.
P values were calculated with univariate logistic regression.

quantitatively analysed, with the 75th percentile CT attenuation value and entropy considered as independent predictors of IAC (odds ratio (OR) = 1.04, 95% CI: 1.01–1.96, P = 0.04 and OR = 3.40, 95% CI: 2.05–5.64, P < 0.01, respectively). The AUC was 0.780 (95% CI 0.711–0.849, P < 0.01). Another study by Chae et al. [15] retrospectively analysed the value of texture features for distinguishing IAC from preinvasive nodules appearing as part-solid GGNs on CT images. Features were quantitatively extracted from 86 cases were used to build a diagnostic model using logistic regression and artificial neural networks, which had an AUC of 0.981 and a 95% CI ranging from 0.973 to 0.987. Therefore, texture features extracted from unenhanced CT images are considered potential factors for aiding in differentiating between IAC and AIS/MIA.

To distinguish between IAC and AIS/MIA appearing as GGNs, texture features extracted from unenhanced CT images have been evaluated frequently in previous studies. However, features from contrast-enhanced CT images are less commonly reported.

In the model generated for this study, the sensitivity, specificity, and AUC were 84.6%, 76.2% and 0.868 (95% CI 0.750–0.986), respectively. Three texture features extracted from enhanced CT images varied significantly between IAC and AIS/MIA; "Uniformity", "GLCMEnergy" and "Volume". There were no significant differences between the two models. The proposed explanation for this finding is that GGNs possess minimal vascular infiltration on histopathology [12]. Furthermore, vessels passing through the lesion were excluded in the segmentation of the ROI. Moreover, the gas content in GGNs is also offset by the addition of contrast agents. With these findings, it was concluded that the administration of contrast-enhanced CT imaging cannot improve the texture differentiation of GGNs over non-enhanced imaging. What's more, Dennie et al. [22] showed that the sensitivity of a model established with three features extracted from enhanced CT images as

Table 2
The performance of models based on selected features for diagnosing invasive adenocarcinoma with GGNs.

Characteristic	AUC	Sensitivity	Specificity	95% CI	Cut-off value
Unenhanced CT					
MedianIntensity	0.770	76.9%	76.2%	[0.621,0.932]	−0.461
Uniformity	0.802	100%	57%	[0.656,0.949]	0.037
GLCMEnergy	0.842	76.9%	85.9%	[0.700,0.984]	−0.119
AngularSecondMoment	0.835	84.6%	71.4%	[0.699,0.972]	−0.145
Volume	0.842	61.5%	95.2%	[0.707,0.978]	−0.725
Combination	0.890	84.6%	76.2%	[0.784,0.996]	0.659
Enhanced CT					
Uniformity	0.795	100%	57%	[0.646,0.944]	0.080
GLCMEnergy	0.813	84.6%	71.4%	[0.661,0.965]	−0.391
Volume	0.835	61.5%	95.2%	[0.696,0.974]	−0.702
Combination	0.868	84.6%	76.2%	[0.750,0.986]	0.612

Note: The combined models were based on selected features by using multivariate logistic regression. All others were calculated with univariate logistic regression.
AUC: area under the receiver operating characteristic curve.
95% CI: 95% confidence interval.

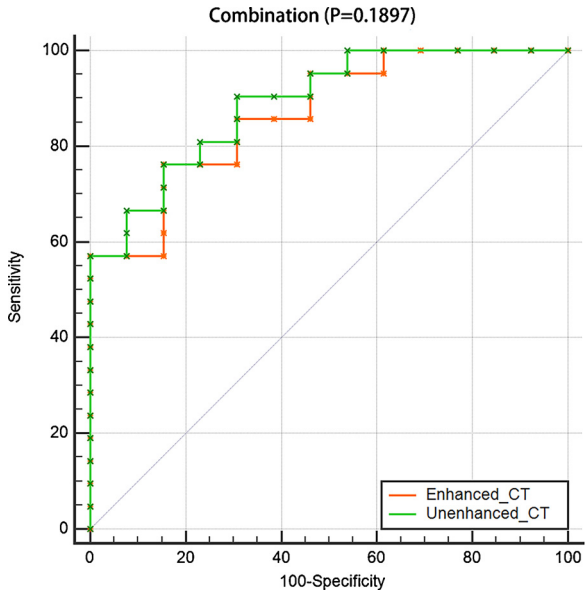

Fig. 3. Receiver operating characteristic (ROC) curve for distinguishing IAC from AIS/MIA.
The AUC values, based on the logistic model of unenhanced and enhanced CT image parameters, were 0.890 and 0.868, respectively.

opposed to non-enhanced CT images decreased from 88% to 38% for differentiating between primary lung tumors and granulomatous lung lesions. This difference was primarily attributed to the presence of contrast agents obscuring the texture of the lesion [23].

Interestingly, dual-energy CT (DECT), which utilizes iodine-enhanced imaging metrics, was shown to better distinguish invasive adenocarcinoma from AIS or MIA compared with virtual non-enhanced images [24]. However, the vast majority of clinical practices still rely on single-energy CT scanners.

Despite the findings in this study, several limitations are worth noting. Firstly, the small sample size may not reflect the overall disease characteristic of AIS, MIA or IAC [25–27]. Furthermore, it may be rare for patients with GGNs to undergo enhanced CT scans in clinical practice, and unenhanced CTs may be used during follow-up. Moreover, to reduce the impact of confounding factors, we relied solely on thin-section non-enhanced and enhanced CT performed at the same time. This strict inclusion and exclusion criteria meant that only 34 GGNs were included as viable for the study. An increased number of cases needs to be included in future studies. Additionally, the reconstruction kernels of enhanced and non-enhanced CT images were different and may have affected the values of texture features. Our study used an FC51 reconstruction kernel for unenhanced CT images and an FC13 reconstruction kernel for enhanced CT images. The results of the study by Lu et al. [28] indicated that images derived from different scanners may have a significant effect on the results of texture features studies. Yet, differences in slice thickness were found to be a more impactful factor influencing quantitative image analysis than differences in reconstruction algorithms. Despite this, however the differences in the reconstruction algorithms used between non-enhanced and enhanced CT images may not be so easy to resolve. In clinical practice, radiologists are primarily concerned with the status of regional lymph node metastasis instead of the enhancement conditions of GGNs on enhanced images. Therefore, different images need different reconstruction algorithms. Finally, manual segmentation of GGN ROIs has more risk of observer bias compared to delineation with semi-automatic regression [29,30]. At present, some semi-automatic segmentation software programs are available. However, the performance of these software programs still needs drastic improvement to produce accurate and reliable results due to the fuzzy boundaries between GGN lesions and the surrounding lung parenchyma.

5. Conclusion

When compared with non-enhanced CT imaging, texture features extracted from contrast-enhanced CT imaging provided no significant benefit in the diagnosis of infiltrative lung adenocarcinoma appearing as GGNs.

Acknowledgements

This work was supported by the Zhejiang Provincial Natural Science Foundation of China (LSY19H180003) and the Medical Health Science and Technology Project of Zhejiang Provincial Health Commission (2019316526).

References

[1] R.L. Siegel, K.D. Miller, A. Jemal, Cancer statistics, 2017, CA Cancer J. Clin. 67 (1) (2017) 7–30, https://doi.org/10.3322/caac.21387.
[2] W.D. Travis, E. Brambilla, M. Noguchi, et al., International Association for the Study of Lung Cancer/American Thoracic Society/European Respiratory Society international multidisciplinary classification of lung adenocarcinoma, J. Thorac. Oncol. 6 (2) (2011) 244–285, https://doi.org/10.1097/JTO.0b013e318206a221.
[3] T. Aoki, Y. Tomoda, H. Watanabe, et al., Peripheral lung adenocarcinoma: correlation of thin-section CT findings with histologic prognostic factors and survival, Radiology 220 (3) (2001) 803–809, https://doi.org/10.1148/radiol.2203001701.
[4] K. Ikeda, K. Awai, T. Mori, K. Kawanaka, Y. Yamashita, H. Nomori, Differential diagnosis of ground-glass opacity nodules: CT number analysis by three-dimensional computerized quantification, Chest 132 (3) (2007) 984–990, https://doi.org/10.1378/chest.07-0793.
[5] K. Kodama, M. Higashiyama, H. Yokouchi, et al., Natural history of pure ground-

glass opacity after long-term follow-up of more than 2 years, Ann. Thorac. Surg. 73 (2) (2002) 383–386.
[6] W.D. Travis, K. Garg, W.A. Franklin, et al., Evolving concepts in the pathology and computed tomography imaging of lung adenocarcinoma and bronchioloalveolar carcinoma, J. Clin. Oncol. 23 (14) (2005) 3279–3287, https://doi.org/10.1200/JCO.2005.15.776.
[7] H.Y. Lee, K.S. Lee, Ground-glass opacity nodules: histopathology, imaging evaluation, and clinical implications, J. Thorac. Imaging 26 (2) (2011) 106–118, https://doi.org/10.1097/RTI.0b013e3181fbaa64.
[8] J. Collins, E.J. Stern, Ground-glass opacity at CT: the ABCs, AJR Am. J. Roentgenol. 169 (2) (1997) 355–367, https://doi.org/10.2214/ajr.169.2.9242736.
[9] D.P. Naidich, A.A. Bankier, H. MacMahon, et al., Recommendations for the management of subsolid pulmonary nodules detected at CT: a statement from the Fleischner Society, Radiology 266 (1) (2013) 304–317, https://doi.org/10.1148/radiol.12120628.
[10] S.M. Lee, C.M. Park, J.M. Goo, H.-J. Lee, J.Y. Wi, C.H. Kang, Invasive pulmonary adenocarcinomas versus preinvasive lesions appearing as ground-glass nodules: differentiation by using CT features, Radiology 268 (1) (2013) 265–273, https://doi.org/10.1148/radiol.13120949.
[11] S. Oda, K. Awai, D. Liu, et al., Ground-glass opacities on thin-section helical CT: differentiation between bronchioloalveolar carcinoma and atypical adenomatous hyperplasia, AJR Am. J. Roentgenol. 190 (5) (2008) 1363–1368, https://doi.org/10.2214/AJR.07.3101.
[12] H.Y. Kim, Y.M. Shim, K.S. Lee, J. Han, C.A. Yi, Y.K. Kim, Persistent pulmonary nodular ground-glass opacity at thin-section CT: histopathologic comparisons, Radiology 245 (1) (2007) 267–275, https://doi.org/10.1148/radiol.2451061682.
[13] F. Gao, M. Li, Y. Sun, L. Xiao, Y. Hua, Diagnostic value of contrast-enhanced CT scans in identifying lung adenocarcinomas manifesting as GGNs (ground glass nodules), Medicine (Baltimore) 96 (43) (2017) e7742, https://doi.org/10.1097/MD.0000000000007742.
[14] R.J. Gillies, P.E. Kinahan, H. Hricak, Radiomics: images are more than pictures, they are data, Radiology 278 (2) (2016) 563–577, https://doi.org/10.1148/radiol.2015151169.
[15] H.-D. Chae, C.M. Park, S.J. Park, S.M. Lee, K.G. Kim, J.M. Goo, Computerized texture analysis of persistent part-solid ground-glass nodules: differentiation of preinvasive lesions from invasive pulmonary adenocarcinomas, Radiology 273 (1) (2014) 285–293, https://doi.org/10.1148/radiol.14132187.
[16] T. Yagi, M. Yamazaki, R. Ohashi, et al., HRCT texture analysis for pure or part-solid ground-glass nodules: distinguishability of adenocarcinoma in situ or minimally invasive adenocarcinoma from invasive adenocarcinoma, Jpn. J. Radiol. 36 (2) (2018) 113–121, https://doi.org/10.1007/s11604-017-0711-2.
[17] J.Y. Son, H.Y. Lee, K.S. Lee, et al., Quantitative CT analysis of pulmonary ground-glass opacity nodules for the distinction of invasive adenocarcinoma from pre-invasive or minimally invasive adenocarcinoma, PLoS One 9 (8) (2014) e104066, https://doi.org/10.1371/journal.pone.0104066.
[18] A.A. Bankier, H. MacMahon, J.M. Goo, G.D. Rubin, C.M. Schaefer-Prokop, D.P. Naidich, Recommendations for measuring pulmonary nodules at CT: a statement from the Fleischner Society, Radiology 285 (2) (2017) 584–600, https://doi.org/10.1148/radiol.2017162894.
[19] H. Muller, N. Michoux, D. Bandon, A. Geissbuhler, A review of content-based image retrieval systems in medical applications-clinical benefits and future directions, Int. J. Med. Inform. 73 (1) (2004) 1–23, https://doi.org/10.1016/j.ijmedinf.2003.11.024.
[20] S.N. Ondimu, H. Murase, Effect of probability-distance based Markovian texture extraction on discrimination in biological imaging, Comput. Electron. Agric. 63 (1) (2008) 2–12, https://doi.org/10.1016/j.compag.2008.01.007.
[21] T.P. Coroller, P. Grossmann, Y. Hou, et al., CT-based radiomic signature predicts distant metastasis in lung adenocarcinoma, Radiother. Oncol. 114 (3) (2015) 345–350, https://doi.org/10.1016/j.radonc.2015.02.015.
[22] C. Dennie, R. Thornhill, V. Sethi-Virmani, et al., Role of quantitative computed tomography texture analysis in the differentiation of primary lung cancer and granulomatous nodules, Quant. Imaging Med. Surg. 6 (1) (2016) 6–15, https://doi.org/10.3978/j.issn.2223-4292.2016.02.01.
[23] I. Phillips, M. Ajaz, V. Ezhil, et al., Clinical applications of textural analysis in non-small cell lung cancer, Br. J. Radiol. 91 (1081) (2018) 20170267, https://doi.org/10.1259/bjr.20170267.
[24] J.Y. Son, H.Y. Lee, J.-H. Kim, et al., Quantitative CT analysis of pulmonary ground-glass opacity nodules for distinguishing invasive adenocarcinoma from non-invasive or minimally invasive adenocarcinoma: the added value of using iodine mapping, Eur. Radiol. 26 (1) (2016) 43–54, https://doi.org/10.1007/s00330-015-3816-y.
[25] V.H. Tam, S. Kabbara, R.F. Yeh, R.H. Leary, Impact of sample size on the performance of multiple-model pharmacokinetic simulations, Antimicrob. Agents Chemother. 50 (11) (2006) 3950–3952, https://doi.org/10.1128/AAC.00337-06.
[26] Y. Zhang, A. Oikonomou, A. Wong, M.A. Haider, F. Khalvati, Radiomics-based prognosis analysis for non-small cell lung cancer, Sci. Rep. 7 (2017) 46349, https://doi.org/10.1038/srep46349.
[27] R.L. Figueroa, Q. Zeng-Treitler, S. Kandula, L.H. Ngo, Predicting sample size required for classification performance, BMC Med. Inform. Decis. Mak. 12 (2012) 8, https://doi.org/10.1186/1472-6947-12-8.
[28] L. Lu, R.C. Ehmke, L.H. Schwartz, B. Zhao, Assessing agreement between radiomic features computed for multiple CT imaging settings, PLoS One 11 (12) (2016) e0166550, https://doi.org/10.1371/journal.pone.0166550.
[29] R. Thawani, M. McLane, N. Beig, et al., Radiomics and radiogenomics in lung cancer: a review for the clinician, Lung Cancer 115 (2018) 34–41, https://doi.org/10.1016/j.lungcan.2017.10.015.
[30] V. Kumar, Y. Gu, S. Basu, et al., Radiomics: the process and the challenges, Magn. Reson. Imaging 30 (9) (2012) 1234–1248, https://doi.org/10.1016/j.mri.2012.06.010.